Damped oscillations of exciton wave packets in the layered semiconductor GaSe observed by four-wave mixing spectroscopy

H. Tahara, Y. Ogawa, and F. Minami
Department of Physics, Tokyo Institute of Technology, Oh-Okayama 2-12-1, Tokyo 152-8551, Japan
(Received 2 July 2010; revised manuscript received 13 August 2010; published 2 September 2010)

We have observed damped oscillations of the exciton wave packet through spectrally resolved four-wave mixing measurements in a layered semiconductor GaSe, and demonstrated that the four-wave mixing spectroscopy is a powerful tool to observe the wave-packet motion. The wave-packet motion is explained theoretically in terms of the configuration coordinate model, where the adiabatic potential curve is shifted due to the exciton-phonon interaction. We have found that the localization of excitons in a few layers enhances the coupling to acoustic phonons.

DOI: 10.1103/PhysRevB.82.113201 PACS number(s): 78.47.−p, 42.50.Md, 63.20.kk, 78.67.Pt

Recently, real-time observation of coherent transient phenomena in the time scale of molecular or lattice vibrations, such as wave-packet oscillations, has been feasible by employing femtosecond spectroscopic techniques. The oscillation of wave packet on the adiabatic potential curve has been observed in small molecules by using the femtosecond pump-probe spectroscopy.[1,2] Many important aspects of coherent transients and chemical reaction dynamics in molecules have been revealed by such measurements. Instead of molecular vibrations in gases, lattice vibrations, i.e., phonons, play an important role in solids. The wave-packet motion associated with a self-trapped exciton has been observed in strongly coupled localized-exciton-phonon systems, e.g., in alkali halides[3,4] and in quasi-one-dimensional halogen-bridged Pt complexes.[5–7] These investigations have provided important information about lattice relaxations after the exciton generation.

In the same way, we can also expect to observe the oscillation of a weakly localized exciton wave packet on the adiabatic potential curve made by the exciton-phonon interaction in semiconductors. However, such exciton oscillations associated with phonons in semiconductors have not been reported yet to our knowledge. In this Brief Report, we present the experimental demonstration of the exciton wave-packet motion on the adiabatic potential curve in a semiconductor. We applied spectrally resolved (SR) and time-resolved (TR) four-wave mixing (FWM) techniques to layered semiconductor GaSe, where the non-Markovian behavior[8] of the interaction between excitons and phonons has been observed by using the multiwave mixing method.[9] The wave-packet motion has been explained theoretically by the configuration coordinate model.[10]

The FWM measurements were performed on a layered semiconductor GaSe. The resonant energy of the 1*s* exciton is 2.109 eV at helium temperature. The sample temperature was set at 3.4 K in a closed cycle refrigerator. The optical pulses were generated by a frequency doubled optical parametric oscillator (OPO) pumped by a mode-locked Ti:sapphire laser. The wavelength was tuned to the exciton resonance of 588 nm (2.109 eV). The pulse duration was 200 fs and the repetition rate was 76 MHz. The original pulse from the OPO was divided into three pulses. Two of them were used for excitation pulses and the other pulse was used for a reference pulse in the TR-FWM measurements. The first and second excitation pulses in the directions $\boldsymbol{k}_1$ and $\boldsymbol{k}_2$ were sent into the sample with the relative delay time τ measured from the first pulse. In order to exclude the biexciton contribution, the polarizations of the two excitation pulses were adjusted to be cocircular. For the TR-FWM measurements, the FWM signals were detected by using the heterodyne technique. In this technique, the reference pulse and the second excitation pulse were frequency shifted with acoustic optical modulators by ν_1 and ν_2, respectively. And then the FWM signals modulated by $2\nu_2$ in the direction of $2\boldsymbol{k}_2-\boldsymbol{k}_1$ were interfered with the reference pulse. The interference was detected by a photodetector, which was connected to a spectrum analyzer. The FWM signals were detected by tuning the spectrum analyzer to $2\nu_2-\nu_1$. The TR-FWM signals were measured by changing the delay time of the reference pulse relative to the FWM signal. For the SR-FWM measurements, the FWM signals in the direction of $2\boldsymbol{k}_2-\boldsymbol{k}_1$ were spectrally resolved by a monochromator and detected by a photomultiplier tube.

The measured SR-FWM intensities are shown in Fig. 1, where the shift of the spectral peak is clearly observed. By increasing the delay time, the peak energy shifts by 0.48 (τ =0.0 ps) and −0.44 (τ=1.0 ps) meV compared with the peak energy at delay time of 2.8 ps, respectively. The blueshift (from τ=1.0 ps to τ=2.8 ps) is more gradual than the redshift (from τ=0.0 ps to τ=1.0 ps). The oscillation of the spectral peak is a damped one because the shift disappears within one period.

In order to know the real-time evolution after the exciton generation, the TR-FWM measurements were performed at various delay times between the first and second pulses. The FWM signals have Gaussian shapes as shown in Fig. 2. The peak position of the TR-FWM signal is plotted as a function of the delay time τ in the inset of Fig. 2. The FWM signals are observed at twice the delay time 2τ, which are known as the photonecho signals. This result leads to the fact that the time-gated spectra at 2τ can be obtained automatically by using the SR-FWM measurements.

The SR-FWM signal was measured with different total excitation density, which were adjusted to 195, 134 and 66 W/cm^2. Though the resolution of the monochromator was 0.4 meV, the peak energy of the FWM signal was measured with high accuracy by using the Gaussian fitting. The

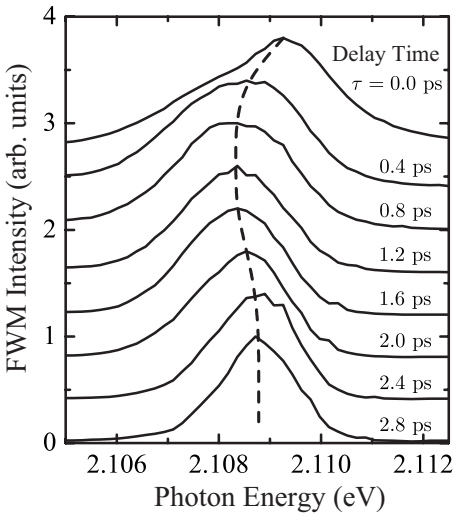

FIG. 1. Normalized spectrally resolved four-wave mixing intensities for various delay time τ with the total excitation density of 195 W/cm^2. The delay time varies from 0.0 to 2.8 ps in 0.4 ps steps as indicated from top to bottom. The dashed line represents the peak-energy shift.

peak-energy shifts are plotted as a function of delay time in Fig. 3, where the peak energy at delay time 1.0 ps (which is the redshift edge energy) is used as the energy reference. The peak-energy shift is density independent as shown in Fig. 3. Therefore, the shift is not explained by the exciton-exciton interaction.

Taking into account the exciton-phonon interaction, the peak-energy shift is explained as the oscillation of the exciton wave packet by the configuration coordinate model. The excitons are treated as the quasi-two-dimensional system because GaSe has a layered structure with stacking disorder.[11,12] Due to the confinement in the c-axis direction, the excitons distort the lattice around themselves. The adiabatic potential curves of the ground state and the exciton state are schematically represented in Fig. 4. As a result of the lattice distortion made by the excitons, the stationary point of the exciton state is shifted for each vibrational mode. The exciton wave packet is made by the excitation light of the exciton resonance energy $\hbar\omega_{eg}$ and oscillates around the stationary point. The exciton wave-packet motion is observed as the ensemble of the vibrational modes, which have their different frequency and stationary points. Hence, the exciton wave packet behaves with destructive interference of several vibrational modes. The motion of the exciton wave

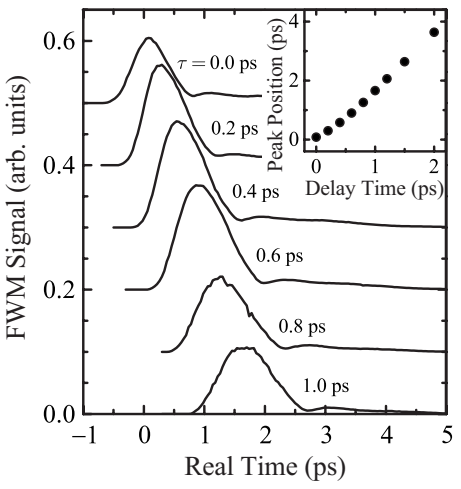

FIG. 2. Time-resolved four-wave mixing amplitudes as a function of real time for various delay time τ with the total excitation density of 134 W/cm^2. The delay time varies from 0.0 to 1.0 ps in 0.2 ps steps as indicated. The zero of the real-time axis is equal to the arrival time of the first excitation pulse. The inset shows the peak position of the signal as a function of delay time.

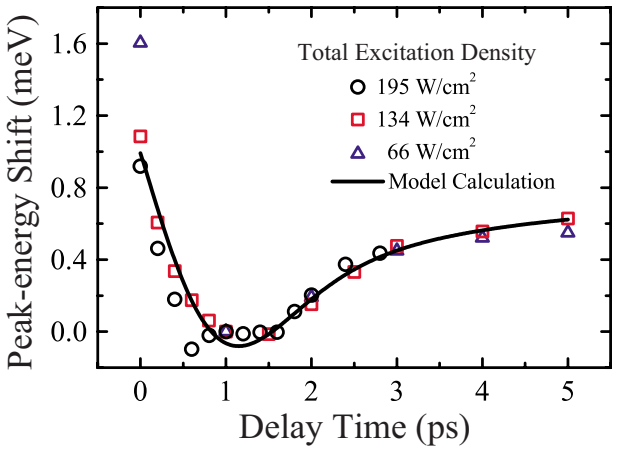

FIG. 3. (Color online) Excitation density dependence of the peak-energy shift as a function of delay time. The plotted data is obtained from the spectrally resolved four-wave mixing signals with the total excitation density of 195, 134 and 66 W/cm^2. The solid line represents the result of the model calculation by using Eq. (11).

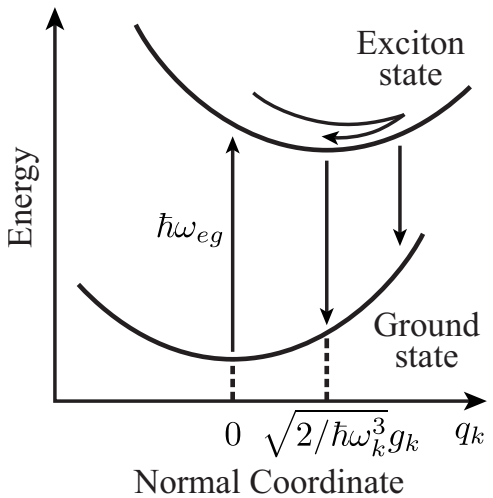

FIG. 4. Adiabatic potential curves for the ground state and the exciton state represented by Eqs. (7) and (8), respectively. The normal coordinate q_k shows the displacement of the nucleus position. After excitation on the stationary point of the ground state (q_k=0) by the exciton resonance light whose energy is expressed as $\hbar\omega_{eg}$, the exciton wave packet oscillates toward the stationary point of the exciton state ($q_k=\sqrt{2/\hbar\omega_k^3}g_k$). The energy difference between both states depends on the position q_k as expressed in Eq. (9).

packet is observed as the time-resolved motion of the spectrum by using FWM measurements, where the emission time is gated at 2τ as shown in Fig. 2.

The optical response of the electron-phonon system has been investigated theoretically.[8,13–16] The total Hamiltonian H_0 is expressed as

$$H_0 = H_{gg}|g\rangle\langle g| + H_{ee}|e\rangle\langle e| \tag{1}$$

with

$$H_{gg} = \sum_k \hbar\omega_k \left(b_k^\dagger b_k + \frac{1}{2} \right), \tag{2}$$

$$H_{ee} = \hbar\omega_{eg} + H_{gg} - V, \tag{3}$$

$$V = \sum_k g_k (b_k + b_k^\dagger), \tag{4}$$

where $|g\rangle$ ($|e\rangle$) is the eigenstate of ground (exciton) state, whose Hermitian conjugate is represented by $\langle g|$ ($\langle e|$), and H_{gg} (H_{ee}) is the eigenvalue of the ground (exciton) state. These eigenvalues are operators in the reservoir variables of the phonon system as written by Eqs. (2) and (3), where $\hbar = h/2\pi$ and h is the Planck constant, ω_{eg} is the exciton resonance frequency and ω_k is the frequency of the phonon mode with wave number k. The annihilation and creation operators of the phonon mode with wave number k are written by $b_k = (\omega_k q_k + i p_k)/\sqrt{2\hbar\omega_k}$ and $b_k^\dagger = (\omega_k q_k - i p_k)/\sqrt{2\hbar\omega_k}$, respectively. In these equations, q_k is the normal coordinate, which represents the displacement of the nucleus position from the lattice point, and its conjugate momentum is represented as p_k.

The exciton-phonon interaction Hamiltonian is represented by V, where we take into account the coupling only in the c-axis direction because the excitons more strongly couple to the phonons involving the vibrations parallel to c axis than the perpendicular vibrations in GaSe.[17] The coupling constant g_k for the deformation potential coupling with longitudinal acoustic (LA) phonons is written by the following:[16]

$$g_k = \sqrt{\frac{\hbar\omega_k}{2\rho u_s^2 \mathcal{V}}} D \int \psi^*(z) e^{ikz} \psi(z) dz, \tag{5}$$

where D is deformation potential constant, ρ is the mass density, u_s is the sound velocity, $\mathcal{V}$ is the normalization volume of phonons, and $\psi(z)$ is the confined exciton wave function at spatial coordinate z, which is parallel to the c axis. The dispersion of acoustic-phonon modes is approximated by the linear relation: $\omega_k = u_s k$. Exciton motion is restricted in quasi-two-dimensional space due to the stacking disorder of layers, therefore the wave function of confined excitons is assumed as $|\psi(z)|^2 \propto \exp[-(z/l)^2]$, in which l is the confinement length of excitons. As the result of z integration, the confinement leads to the distribution: $g_k \propto \sqrt{\omega_k} \exp[-(l\omega_k/2u_s)^2]$. The spectral density $I_{\text{ex-ph}}(\omega)$ is expressed as

$$I_{\text{ex-ph}}(\omega) = \sum_k g_k^2 \delta(\omega - \omega_k) = \alpha^2 \hbar^2 \omega \exp\left[-\frac{l^2\omega^2}{2u_s^2} \right], \tag{6}$$

where $\delta(\omega)$ is the delta function of ω and α is the dimensionless coupling constant. This spectral density is similar to that of the Ohmic reservoir model, where the Gaussian cutoff term in Eq. (6) is replaced with the exponential cutoff term.[18]

In order to express the adiabatic potential curves of the ground (exciton) state W_g (W_e), q_k, and p_k are substituted for b_k and $b_k^\dagger$. Here, W_g and W_e are defined as $W_g = H_{gg} - \Sigma_k p_k^2/2$ and $W_e = H_{ee} - \Sigma_k p_k^2/2$, respectively. By using this substitution, we obtain

$$W_g = \sum_k \frac{1}{2} (\omega_k q_k)^2, \tag{7}$$

$$W_e = \sum_k \frac{1}{2} \left(\omega_k q_k - \sqrt{\frac{2}{\hbar\omega_k}} g_k \right)^2 + \hbar\omega_{eg} - \sum_k \frac{g_k^2}{\hbar\omega_k}. \tag{8}$$

These potential curves are represented by the summation of the harmonic potential curves as a function of each q_k. The stationary point of the harmonic potential curve for each q_k is taken at $q_k = 0$ and $q_k = \sqrt{2/\hbar\omega_k^3} g_k$ for the ground state and the exciton state, respectively. The difference of the stationary point between these states is caused by the exciton-phonon interaction. Each coordinate q_k varies as a function of time t due to the displacement of the nucleus position with the lattice relaxation. The expression $q_k(t)$ is defined as the position of the exciton wave packet projected on the coordinate q_k at the time t. At the time $t=0$, the resonant light generates the exciton wave packet on $q_k = 0$, which is the stationary point of the ground state. Then, the exciton wave packet shifts toward the stationary point of the exciton state ($q_k = \sqrt{2/\hbar\omega_k^3} g_k$) with the oscillation of frequency ω_k as shown in Fig. 4. The oscillation of $q_k(t)$ on the harmonic potential curve W_e is written by

$$q_k(t) = \sqrt{\frac{2}{\hbar\omega_k}} \frac{g_k}{\omega_k} (1 - \cos[\omega_k t + \theta]), \tag{9}$$

where θ is the initial phase of the phonon oscillation. The energy difference $E_{eg}(t)$ at the time t, which is equal to $W_e - W_g$, is obtained by

$$\begin{aligned} E_{eg}(t) &= \hbar\omega_{eg} - \sum_k \frac{2g_k^2}{\hbar\omega_k} (1 - \cos[\omega_k t + \theta]) \\ &= \hbar\omega_{eg} - \int_0^\infty \frac{2}{\hbar\omega} I_{\text{ex-ph}}(\omega) (1 - \cos[\omega t + \theta]) d\omega. \end{aligned} \tag{10}$$

For the FWM measurements, the signals are automatically time gated at twice the delay time 2τ, when the TR-FWM signal is observed as shown in Fig. 2. Therefore, the peak-energy shift for various delay times τ is finally obtained as

$$E_{\mathrm{shift}}(\tau) = 2\alpha^2\hbar \int_0^\infty \exp\left[-\frac{l^2\omega^2}{2u_s^2}\right]\cos[2\omega\tau + \theta]d\omega. \quad (11)$$

We show the result of the model calculation of the peak-energy shift (the redshifted edge energy is used as the energy reference) by using Eq. (11) as a solid line in Fig. 3, which is fitted to the experimental data with the total excitation density of 134 $\mathrm{W/cm^2}$. The parameters are obtained as $l=4.1$ nm, $\alpha=1.3$, and $\theta/\pi=0.47$ through the fitting, where the sound velocity of the LA phonon in GaSe $u_s=2.482\times10^5$ cm/s is used.[19] The localization length $2l$ is corresponding to the length of ten layers because there are two layers in a unit cell which has a lattice constant $c=1.59$ nm.[20] This localization is consistent with the investigations of stacking disorder in GaSe, in which it has been found that the excitons are localized over five to ten layers and that the k-selection rule is broken down by the stacking disorder in the c-axis direction.[11,12] The localization of excitons also plays a significant role in our theoretical analysis, where the k-space broadening causes the damped oscillation.

The exciton-phonon coupling constant α is comparable to 1, which is a typical order for the acoustic deformation potential coupling. The total phonon coupling, however, is enhanced by the confinement in the c-axis direction, which is expected for localized quasi-two-dimensional excitons.[21] Through integration of the spectral density $I_{\text{ex-ph}}(\omega)$, it is found that the enhancement is inversely proportional to l^2. In addition, the coupling strength might be correlated with the ionicity because the III-VI semiconductor GaSe is less polar than the I-VII and II-VI polar semiconductors that are treated as the strongly coupled system.

In summary, we have observed the motion of the exciton wave packet through spectrally resolved four-wave mixing measurements on the layered semiconductor GaSe, which is the observation of the exciton wave-packet motion due to lattice relaxation in semiconductors. The spectral motion is explained theoretically by the configuration coordinate model based on the exciton-phonon interaction. The model calculation leads us to the conclusion that the excitons in GaSe are localized in about ten layers via the acoustic deformation potential coupling and then it takes a few picoseconds to arrive at the stationary point of the lattice deformation. It is a remarkable point that the oscillation of the exciton wave packet is observed in the quasi-two-dimensional system, which has more degrees of freedom than those in reported measurements.[1–7] Since none of the results is almost specific to GaSe, it would be interesting to carry out similar experiments in other layered materials, e.g., GaAs quantum wells where non-Markovian behavior has reported in a few picosecond regime.[22,23]

This work was supported by the Global Center of Excellence Program by MEXT, Japan through the Nanoscience and Quantum Physics Project of the Tokyo Institute of Technology.

[1] T. S. Rose, M. J. Rosker, and A. H. Zewail, J. Chem. Phys. **88**, 6672 (1988).
[2] S. Mukamel, *Principles of Nonlinear Optical Spectroscopy* (Oxford University Press, New York, 1995).
[3] T. Tokizaki, T. Makimura, H. Akiyama, A. Nakamura, K. Tanimura, and N. Itoh, Phys. Rev. Lett. **67**, 2701 (1991).
[4] A. L. Shluger and K. Tanimura, Phys. Rev. B **61**, 5392 (2000).
[5] S. Tomimoto, S. Saito, T. Suemoto, K. Sakata, J. Takeda, and S. Kurita, Phys. Rev. B **60**, 7961 (1999).
[6] T. Matsuoka, J. Takeda, S. Kurita, and T. Suemoto, Phys. Rev. Lett. **91**, 247402 (2003).
[7] Y. Takahashi, K. Yasukawa, S. Kurita, and T. Suemoto, Phys. Rev. B **81**, 081102(R) (2010).
[8] M. Aihara, Phys. Rev. B **25**, 53 (1982).
[9] T. Kishimoto, A. Hasegawa, Y. Mitsumori, J. Ishi-Hayase, M. Sasaki, and F. Minami, Phys. Rev. B **74**, 073202 (2006).
[10] Y. Toyozawa, *Optical Processes in Solids* (Cambridge University Press, Cambridge, England, 2003).
[11] J. J. Forney, K. Maschke, and E. Mooser, J. Phys. C **10**, 1887 (1977).
[12] V. Capozzi and K. Maschke, Phys. Rev. B **34**, 3924 (1986).
[13] Y. Toyozawa, A. Kotani, and A. Sumi, J. Phys. Soc. Jpn. **42**, 1495 (1977).
[14] Y. Kayamura, J. Phys. Soc. Jpn. **57**, 292 (1988).
[15] M. Hama and M. Aihara, Phys. Rev. B **38**, 1221 (1988).
[16] E. A. Muljarov and R. Zimmermann, Phys. Rev. Lett. **93**, 237401 (2004).
[17] M. Schlüter, Nuovo Cimento B **13**, 313 (1973).
[18] M. Sasaki, A. Hasegawa, J. Ishi-Hayase, Y. Mitsumori, and F. Minami, Phys. Rev. B **71**, 165314 (2005).
[19] Kh. M. Khalilov and K. I. Rzaev, Kristallografiya **11**, 929 (1966) [Sov. Phys. Crystallogr. **11**, 786 (1967)].
[20] S. Jandl, J. L. Brebner, and B. M. Powell, Phys. Rev. B **13**, 686 (1976).
[21] I. V. Bondarev, S. A. Maksimenko, G. Ya. Slepyan, I. L. Krestnikov, and A. Hoffmann, Phys. Rev. B **68**, 073310 (2003).
[22] Y. Ogawa and F. Minami, Phys. Rev. B **75**, 073302 (2007).
[23] S. G. Carter, Z. Chen, and S. T. Cundiff, Phys. Rev. B **76**, 121303(R) (2007).